Particuology 115 (2026) 35–46

Contents lists available at ScienceDirect

Particuology

journal homepage: www.elsevier.com/locate/partic

Elucidation of the dispersion characterization of lithium-ion battery slurry under effects of both composite conductive agent amount and carbon nanotubes to graphene mass ratio

Zhilong Wang[a], Bingjia Li[a], Xiao Yang[a], Jianhang Lu[a], Jiatan Zhang[a], Chunguo Zhou[a], Irfan Bahiuddin[b], Bo Sun[a], Tong Zhao[a,c,*]

[a] Faculty of Mechanical and Precision Instrument Engineering, Xi'an University of Technology, Xi'an, 710048, China
[b] Department of Mechanical Engineering, Universitas Gadjah Mada, Yogyakarta, 55281, Indonesia
[c] Key Laboratory of Green and Intelligent Development and Efficient Utilization of Strategic Mineral Resources of Xinjiang Production and Construction Corps, Faculty of Electromechanical and Automation, Xinjiang University of Technology, Hotan City, 848000, China

HIGHLIGHTS

- $LiCoO_2$ particles are well dispersed within LIB slurry when $\varphi_{com2} = 0.5\%$.
- Both $LiCoO_2$ particles and the composite conductive agent are well dispersed to form network when m_{CNTS}: $m_{Gr} = 4{:}1$.
- The best synergistic effect between CNTs and Gr provides a solid foundation for LIB production.

GRAPHICAL ABSTRACT

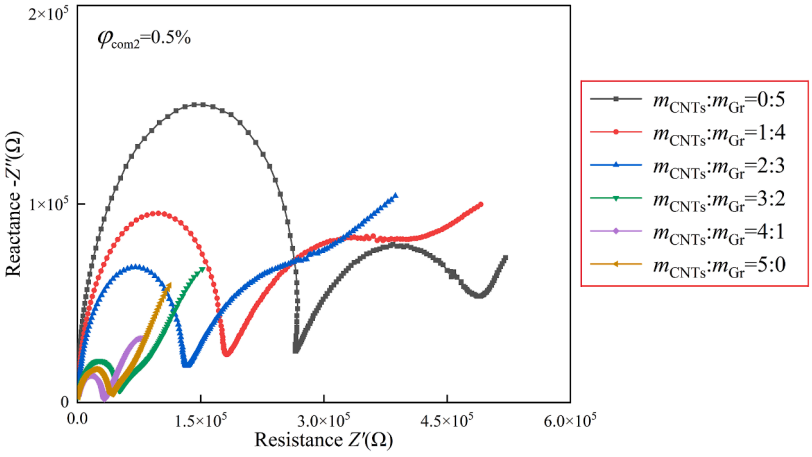

ARTICLE INFO

Keywords:
Composite conductive agent
Lithium-ion battery slurry
Carbon nanotubes
Graphene

ABSTRACT

This manuscript mainly proposed an effective method to well disperse the composite conductive agent which is composed of carbon nanotubes (CNTs) and graphene (Gr) in lithium-ion battery (LIB) slurry. Electrochemical Impedance Spectroscopy (EIS), Scanning Electron Microscopy (SEM) and gravitational sedimentation (GS) are employed to characterize the electrochemical, morphological and stability characterizations of LIB slurry, respectively. Specifically, electrochemical characterizations of LIB electrode slurries are performed by fitting Nyquist plots with a 10-parameter EEC, and quantitative morphological analysis of SEM images is conducted using a Mask R-CNN instance segmentation algorithm, both of which were proposed in our prior published research works. Consequently, the dispersion characterizations of LIB slurry are able to be summarized as

* Corresponding author. Faculty of Mechanical and Precision Instrument Engineering, Xi'an University of Technology, Xi'an, 710048, China.
E-mail address: tongzhao@xaut.edu.cn (T. Zhao).

https://doi.org/10.1016/j.partic.2026.05.006
Received 24 March 2026; Received in revised form 8 May 2026; Accepted 11 May 2026
Available online 17 May 2026

follows: $LiCoO_2$ particles are well dispersed in LIB slurry at $\varphi_{com2} = 0.5\%$, by contrast, the composite conductive agent achieves superior coating and networking of $LiCoO_2$ particles under the conditions of both $\varphi_{com2} = 0.5\%$ and m_{CNTs}:m_{Gr} = 4:1, due to the maximized CNTs-Gr synergistic effect. Meanwhile, the formed three-dimensional "long-range" conductive network maintains the stability of its internal skeleton structure during the sedimentation of LIB slurry. This finding holds significant potential to advance the application of CNTs/Gr composite conductive agents in LIB slurry.

1. Introduction

With the rapid development of society and the economy, electronic products powered by lithium-ion batteries (LIBs) have become increasingly popular among consumers, in contrast to traditional electronics that rely on non-renewable energy sources such as coal, oil, and natural gas for power supply (Chen et al., 2026; Zheng et al., 2025). However, the performance LIB is usually limited to a certain extent by the content of conventional single conductive additives in LIB slurry (Zeng et al., 2025). Specifically, a low content of conventional single conductive additive fails to form an effective conductive network, since the active material surface cannot be fully covered by the composite of conductive additives and binder. Conversely, an excessive content of such single conductive additives can lead to serious particle agglomeration, thereby destroying the conductive network (Cao et al., 2023). Therefore, how to construct an ideal conductive network in LIB slurry with the minimal dosage of conductive additives constitutes the key to maximizing the overall electrochemical performance of LIBs.

Accordingly, as an alternative to conventional single conductive additives, composite conductive agent composed of carbon nanotubes (CNTs) and graphene (Gr) has gained growing prominence in the fabrication of LIBs. Shen et al. used a solution-based method to construct a highly conductive 3D hierarchical network structure by growing TiO_2 particles on the surfaces of Gr and CNTs for rapid lihtium storage. Such structural merits can be attributed to two key factors: firstly, TiO_2 nanoparticles are uniformly dispersed on CNTs and Gr; secondly, the interlaced CNTs are intimately embedded or attached onto Gr sheets to form 3D conductive networks (Shen et al., 2011). Lei et al. synthesized a three-dimensional $LiFePO_4$ (LFP)-CNTs-Gr composite cathode via a solid-state reaction, demonstrating that the synergistic effect of CNTs and Gr constructs an efficient 3D conductive network that accelerates electron transfer and Li + diffusion, enabling the material to deliver 168.9 mAh/g at 0.2 C and 115.8 mAh/g at 20 C with superior high-rate performance (Lei et al., 2015). Subsequently, Chen et al. further verified this conclusion by synthesizing the LFP-CNTs-Gr composite cathode via a hydrothermal method (Chen et al., 2018). Zhang et al. successfully synthesized a highly interconnected 3D nitrogen-doped reduced hydroxylated CNTs-Gr composite aerogel for photovoltaic devices, they found that this material shows great promise for the construction of low-cost, metal-free, flexible counter electrodes with excellent performance (Zhang et al., 2016). Wang et al. fabricated a SnO_2/CNTs-Gr nanosheet aerogel composite with 3D conductive framework for the anode of LIB, they pointed out that the fabricated composite exhibits a very decent cycling stability and an excellent rate capability (Wang et al., 2017). Zhang et al. developed a three-dimensional porous CNTs-Gr network loaded with micro-nano structured $FeF_3{\cdot}0.33H_2O$, which acts as a high volumetric performance cathode for LIB, demonstrating excellent rate capability and high mass loading tolerance, with a discharge capacity of 162 mAh/g at 1 C and 92% capacity retention when the areal mass loading increases from 1 to 5 mg/cm (Zhang et al., 2020). An et al. also fabricated a three-dimensional porous silicon/CNTs-Gr for the anode of LIB, which can provide short pathways for electrons, conductive transport highways for Li^+, a sufficient interface for contact of the electrolyte and electrode, and an effective buffer matrix to alleviate structural change during discharge/charge cycling (An et al., 2020). Ding et al. developed a holey reduced graphene oxide (h-GO)/CNTs composite conductive network with $LiMn_{0.7}Fe_{0.3}PO_4$ as a cathode material for LIB, demonstrating that the cathode delivers 112 mAh g^{-1} at 20 C, which far exceeds the 35 mAh/g of conventional GO/CNTs-based electrodes and significantly improves the high-rate performance of LIB (Ding et al., 2020). Kim et al. designed a hierarchical LFP/CNTs/Gr quantum dots (GQDs) composite cathode that delivers outstanding rate capability up to 20 C and excellent long-cycle stability via the synergistic conduction of CNTs, showing substantially improved electrochemical performance over conventional carbon-based LFP electrodes (Kim et al., 2023). Liu et al. constructed a 3D hybrid structured Gr aerogel composite for the anode of LIB, namely, one-dimensional CNTs cross-linked Gr aerogels to form porous 3D aerogel skeleton and active materials dispersed on the surface of nitrogen doped CNTs, which has a significant promoting effect on the improvement of LIB electrochemical performance (Liu et al., 2023). Liu et al. systematically investigated ternary nanocarbon conductive networks, demonstrating that monodispersed CNTs form an efficient "plane-to-line-to-point" conducting mode with Gr and LFP, which constructs both short and long-range electronic conduction and open ion channels, enabling the LFP cathode to achieve excellent rate performance even at a low CNTs loading (Liu et al., 2022). However, the above-mentioned research works only focused on the integration of CNTs and Gr with different materials including LFP, TiO_2 and SnO_2 to construct electrode materials for LIB. Obviously, the application of both CNTs and Gr in $LiCoO_2$-based active material remains unclear. To fill this research gap, it is an urgent need to focus on the research of CNTs and Gr applied to $LiCoO_2$ in LIB slurry.

At the present work, the influences of both the composite conductive agent which is composed of CNTs and Gr amount and CNTs to Gr mass ratio on the dispersion characterizations of LIB slurry are clarified by using the following three methods which are EIS, Scanning Electron Microscopy (SEM) and gravitational sedimentation (GS). Herein, EIS as a powerful tool has the ability to measure the dielectric properties of materials and interfaces (Fan & Fedkiw, 1998), which is then used to characterize the frequency-dependent responses of LIB slurry. Moreover, SEM as a core microscopic tool has the ability to visually observe internal micro topography in LIB slurry, which is then used to provide key microscopic evidence for evaluating LIB slurry dispersion (Ikeno et al., 2022). Furthermore, GS as a straightforward analytical approach has the ability to observe and quantify the settling dynamics of particles in suspensions, which is then used to assess the dispersion stability of LIB slurry. The purpose of this research work is to obtain the optimal composite method of the composite conductive agent composed of CNTs and Gr and explore its dispersion characteristics in LIB slurry, which has great potential to enhance the final performance of LIBs.

2. Experiment procedures

2.1. Experimental setup

Fig. 1 illustrates the experimental setup. Specifically, in Fig. 1(a), the material drying equipment includes laboratory dryer and precision electronic scale. In Fig. 1(b), the slurry mixing system contains mortar, beaker and mixer. Moreover, Fig. 1(c) shows the EIS measurement system, which includes an impedance spectroscopy analyzer, two aluminum electrodes, and a pair of four-terminal probes equipped with Kelvin clamps, a personal computer (PC), and an anti-static pad. A pair of aluminum electrodes is affixed to the inner walls of the beaker that

holds the slurry samples. A set of Kelvin clamps is fastened between these two electrodes. The electrochemical signals emitted by the slurry samples are detected by the four-terminal probes clamped to the electrodes. Following acquisition, measured data are transferred to the computer for subsequent processing, and the anti-static pad is incorporated to mitigate the influence of external static electricity on measurement accuracy. Fig. 1(d) displays the SEM system (Zeiss Sigma 500), while Fig. 1(e) details the gravitational sedimentation (GS) apparatus, which uses a 10 mL graduated cylinder.

2.2. Experimental materials and conditions

Materials used in this work include CNTs, Gr, lithium cobalt oxide ($LiCoO_2$), N-methyl-2-pyrrolidone (NMP) and polyvinylidene fluoride (PVDF). Specifically, the composite conductive agent composed of CNTs and Gr enhances the electronic conductivity of LIB slurry, as the active material $LiCoO_2$ exhibits lower intrinsic conductivity of 10^{-3} S/cm. NMP is utilized as a solvent to dissolve PVDF for the preparation of a homogeneous PVDF-NMP solution. As a polymeric binder, PVDF demonstrates outstanding electrochemical stability and excellent adhesion to electrode materials as well as current collectors.

In accordance with the research purposes, the experimental conditions are outlined as follows: Table 1 lists mass fractions of each component in LIB slurry. Specifically, the mass of $LiCoO_2$ was fixed at 35.2 g, the total mass fraction of composite conductive agent is assigned four distinct values: $\varphi_{com1} = 0.3\%$, $\varphi_{com2} = 0.5\%$, $\varphi_{com3} = 0.7\%$, and $\varphi_{com4} = 0.9\%$. Simultaneously, six distinct mass ratios of CNTs to Gr (m_{CNTs}:m_{Gr}) were employed for each loading of the composite conductive agent, which are 0:5, 1:4, 2:3, 3:2, 4:1 and 5:0. Therefore, a total of 24 LIB slurry samples were prepared. Secondly, according to our previously published method for optimizing the conductive agent composite (Wang et al., 2025b), the mixing parameters were fixed as follows: the binary composite conductive solution was mixed at a rotational speed of $n_1 = 1320$ rpm for $t_1 = 5$ min. Thereafter, when this binary conductive solution was blended with $LiCoO_2$ slurry to fabricate LIB slurry, the corresponding stirring speed and time were adjusted to $n_2 = 1320$ rpm and $t_2 = 6$ min, respectively. Detailed mass fractions of individual components in LIB slurry are provided in Table 1. Concurrently, Table 2 lists the key experimental information: the mass fraction of composite conductive agent φ_{com}, the mass ratio of CNTs to Gr m_{CNTs}:m_{Gr} and the associated mass values for each ratio. Furthermore, in terms of the experimental setup for GS, the liquid level height of LIB slurry was measured with a vernier caliper to guarantee measurement accuracy. Meanwhile, the sedimentation process of all LIB slurries was performed in graduated cylinders within a sealed environment. This design not only avoids the evaporation of NMP solvent but also eliminates complex physical behaviors such as weight gain induced by water absorption.

Table 1
Mass values of each component in LIB slurry.

Experimental material	Category	Mass values (g)
Lithium cobalt oxide ($LiCoO_2$)	Active material	35.2
Composite conductive agent (CNTs and Gr)	Conductive agent	0.11, 0.18, 0.26, 0.33
Poly vinylidene fluoride (PVDF)	Binder	1.6
N-Methylpyrrolidone (NMP)	Organic Solvent	38.4

Table 2
Detailed information on the amount of composite conductive agent φ_{com}, the mass ratio of CNTs to Gr m_{CNTs}:m_{Gr} and the corresponding mass values for each m_{CNTs}:m_{Gr}.

Composite conductive agent amount	CNTs to Gr mass ratio m_{CNTs}:m_{Gr}	Corresponding mass values for each m_{CNTs}:m_{Gr}
$\varphi_{com1} = 0.3\%$	0:5, 1:4, 2:3, 3:2, 4:1, 5:0	0:0.11, 0.02:0.09, 0.04:0.07, 0.07:0.04, 0.09:0.02, 0.11:0
$\varphi_{com2} = 0.5\%$	0:5, 1:4, 2:3, 3:2, 4:1, 5:0	0:0.18, 0.04:0.14, 0.07:0.11, 0.11:0.07, 0.14:0.04, 0.18:0
$\varphi_{com3} = 0.7\%$	0:5, 1:4, 2:3, 3:2, 4:1, 5:0	0:0.26, 0.05:0.21, 0.1:0.16, 0.16:0.1, 0.21:0.05, 0.26:0
$\varphi_{com4} = 0.9\%$	0:5, 1:4, 2:3, 3:2, 4:1, 5:0	0:0.33, 0.07:0.26, 0.13:0.2, 0.2:0.13, 0.26:0.07, 0.33:0

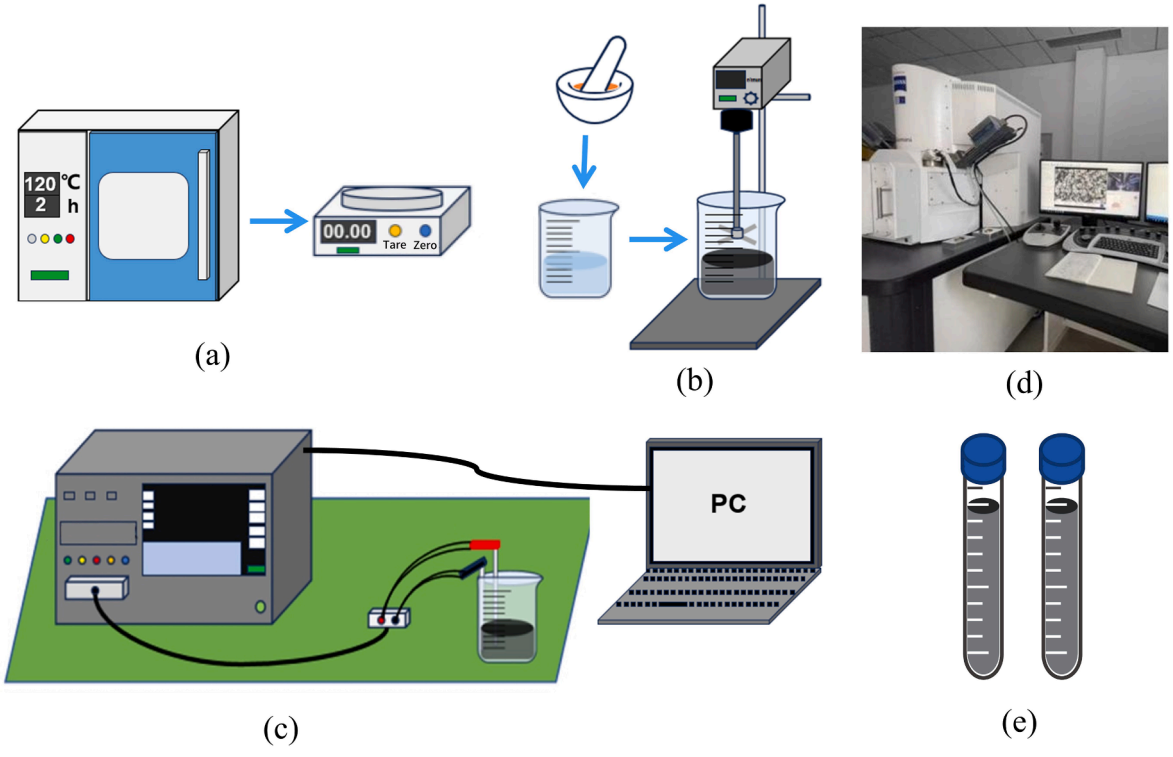

Fig. 1. Experimental setup: (a) Material drying equipment; (b) Slurry mixing system; (c) EIS measurement system; (d) SEM measurement system; (d) GS equipment.

Accordingly, the weight of LIB slurries remains unchanged throughout the entire GS test, which further enhances the accuracy and reliability of the GS experimental method.

2.3. Experimental methods

Three different methods which are EIS, SEM and gravitational sedimentation (GS) are used to characterize the dispersion characterizations of LIB slurry. The specific measurement methods are as follows: firstly, before performing EIS experiments, the measuring apparatus was calibrated by means of open-circuit and short-circuit corrections to remove systematic errors. Subsequently, an excitation current with an average amplitude of 0.5 mA is injected, while the frequency was scanned over the range of 4 Hz to 5 MHz. In total, 201 data points were sampled within this range to construct Nyquist and Bode plots. Meanwhile, as is shown in Fig. 2, a previously proposed 10-parameter electrical equivalent circuit for LIB slurry is used to fit the Nyquist plots of EIS measurement data (Wang et al., 2017a). Herein, R_{CM} refers to charge moving resistance, R_{SO} refers to PVDF-NMP solution resistance, C_{SO} refers to PVDF-NMP solution capacitance, R_P refers to guiding electrical path resistance, R_{dl} refers to PVDF-composite conductive agent double-layer resistance, C_{dl} refers to PVDF-composite conductive agent double-layer capacitance, both CPE_P and CPE_{dl} are constant phase angle elements. Thereafter, SEM experimental observations were conducted under a magnification of 1000× and an acceleration voltage of 10 kV. Thirdly, in the GS experiments, each LIB slurry sample was evaluated under the standardized conditions with a constant volume of 15 mL and a fixed initial height denoted as (H_0). Meanwhile, the GS experiment was continuously monitored and documented throughout a 7-day duration, after which the stability of LIB slurry was assessed using the final average sedimentation rate (V) and sedimentation ratio (Y). The complete experimental process is schematically shown in Fig. 3.

During the preparation of LIB slurry, all raw materials were pre-dried to eliminate residual moisture. This is essential to prevent adverse effects on the accuracy of subsequent weighing and the reliability of experimental measurements. Specifically, both $LiCoO_2$ particles (as the active material) and PVDF powder (as the binder) are mixed, placed in a high-temperature resistant beaker, and baked in a constant-temperature blast drying oven at 120 °C for 2 h to remove as much moisture as possible that the powders have absorbed from the air. Meanwhile, CNTs and Gr were individually loaded into two distinct beakers and thermally treated in an oven at 180 °C for 3 h. Afterwards, CNTs and Gr were premixed in NMP solvent to form a binary conductive solution. Then, NMP was added in three portions with ratios of 1/5, 2/5, and 2/5 to the mortar containing pre-dried PVDF to form a PVDF-NMP solution. Moreover, the binary conductive solution and the PVDF-NMP solution were manually premixed for 10 s to form a binary composite conductive solution. Furthermore, $LiCoO_2$ particles were added to the binary composite conductive solution; meanwhile, mechanical mixing was performed to obtain the LIB slurry with the composite conductive agent CNTs/Gr. Eventually, the prepared LIB slurries were characterized by using EIS, SEM and GS measurements. All aforementioned experiments were conducted in triplicate, and the final results were reported as the average of three independent tests to eliminate measurement errors.

3. EIS experimental results

3.1. Results of LIB slurry with composite conductive agent amount

Fig. 4 shows the Nyquist plots and Bode plots of the LIB slurry under four different composite conductive agent amount which are $\varphi_{com1} = 0.3\%$, $\varphi_{com2} = 0.5\%$, $\varphi_{com3} = 0.7\%$, $\varphi_{com4} = 0.9\%$. In Fig. 4(a), it is clear that two semi-circles are appeared for each composite conductive agent amount. Specifically, the diameter of the semi-circle in low frequency range is firstly decreased and then increased with the increase of composite conductive agent amounts. Meanwhile, the variation trend of the semi-circle diameter in high frequency range is consistent with that in low frequency range. Herein, the diameter of the semi-circle in both low and high frequency ranges in the case of $\varphi_{com2} = 0.5\%$ is smaller than that of other cases including $\varphi_{com1} = 0.3\%$, $\varphi_{com3} = 0.7\%$ and $\varphi_{com4} = 0.9\%$. This shows that LIB slurry has smaller impedance in the case of $\varphi_{com2} = 0.5\%$. Moreover, when the dosage of composite conductive agent is reduced to $\varphi_{com1} = 0.3\%$, the inadequate additive content fails to fully wrap partial $LiCoO_2$ particles via the conductive agent - PVDF composite layer. Consequently, the exposure degree of $LiCoO_2$ grains is significantly elevated. Furthermore, when the loading of composite conductive agent is increased to $\varphi_{com4} = 0.9\%$, the excessive conductive additive enables full surface coverage of particles by the conductive agent - PVDF composite network. However, excessive dosage also induces severe agglomeration driven by intrinsic van der Waals intermolecular forces. (Liu et al., 2007). Hence, based on the analysis of the two aforementioned scenarios, it can be observed that either excessive or insufficient amounts of the composite conductive agent are able to increase both the resistance and reactance of the LIB slurry. Additionally, in Fig. 4(b), the peak frequency $f_{peak,\ high}$ defined as the frequency of $LiCoO_2$-NMP interface dispersion can be clearly observed, which is a measure of the time required for charges in electrolyte solution to recover their equilibrium distribution after ceasing an external perturbation (Wang et al., 2017b; 2019; 2025b). However, since the variation trend of $f_{peak,\ high}$ in Fig. 4(b) is indistinct. For clear comparison, the extracted $f_{peak,\ high}$ values are further summarized in Fig. 5. As illustrated, the sample with $\varphi_{com2} = 0.5\%$ exhibits a higher $f_{peak,\ high}$ than the other cases including $\varphi_{com1} = 0.3\%$, $\varphi_{com3} = 0.7\%$ and $\varphi_{com4} = 0.9\%$. This illustrated that the time required for charges to recover their equilibrium distribution in the case of $\varphi_{com2} = 0.5\%$ is shorter than that in other cases including $\varphi_{com1} = 0.3\%$, $\varphi_{com3} = 0.7\%$ and $\varphi_{com4} = 0.9\%$. Therefore, a conductive network structure is formed in LIB slurry in the case of $\varphi_{com2} = 0.5\%$.

Using our previously proposed 10-parameter electrical equivalent circuit to fit the Nyquist plots of LIB slurries, this work systematically analyzes the electrochemical characterizations of samples with four composite conductive agent loadings: $\varphi_{com1} = 0.3\%$, $\varphi_{com2} = 0.5\%$,

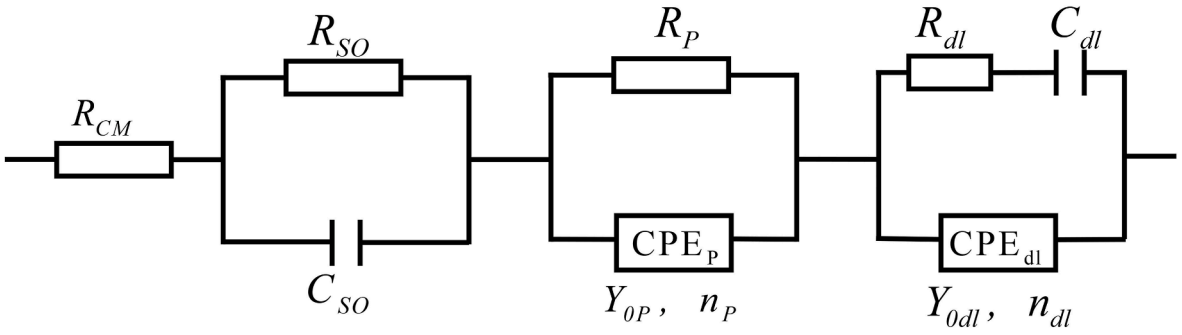

Fig. 2. The 10-parameter electrical equivalent circuit (Wang et al., 2017a).

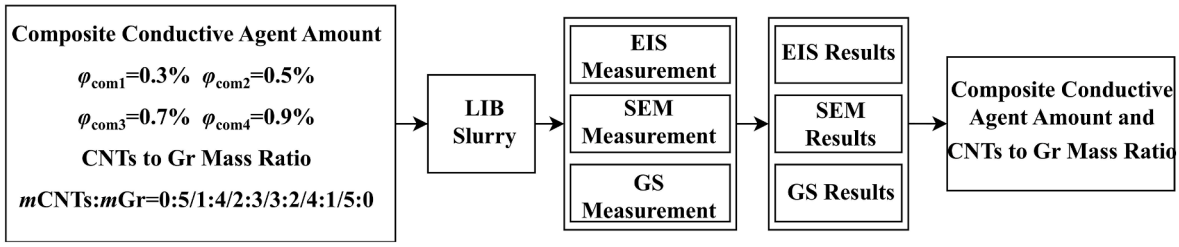

Fig. 3. Process to obtain optimal composite conductive agent content and CNTs to Gr mass ratio in LIB slurry.

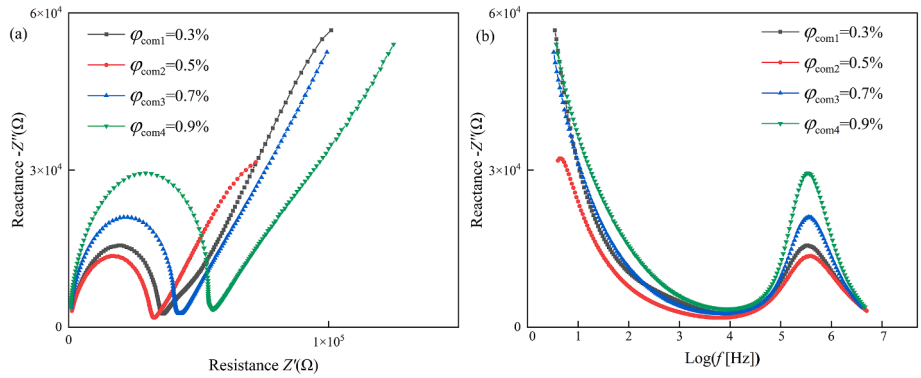

Fig. 4. EIS results of LIB slurry under four different composite conductive agent amounts which are $\varphi_{com1} = 0.3\%$, $\varphi_{com2} = 0.5\%$, $\varphi_{com3} = 0.7\%$, $\varphi_{com4} = 0.9\%$ (a) Nyquist plots (b) Bode plots.

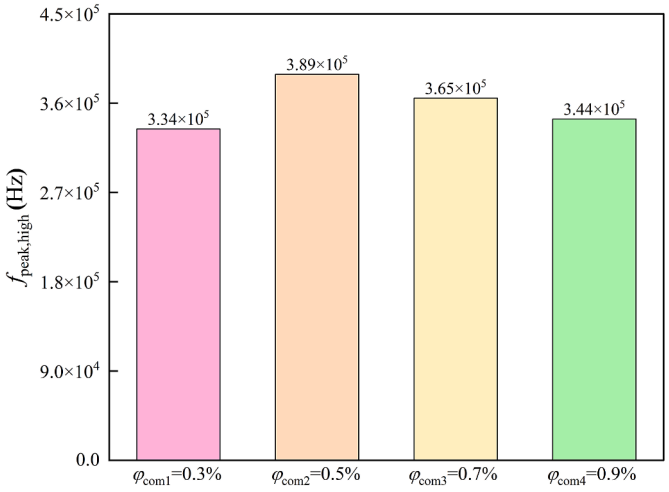

Fig. 5. Peak frequency in the high frequency range $f_{peak,\ high}$ obtained from Fig. 4(b).

$\varphi_{com3} = 0.7\%$ and $\varphi_{com4} = 0.9\%$. As is shown in Fig. 6, EIS fitting results can be observed. In Fig. 6(a), with the increase of the amount of composite conductive agent, the resistance of PVDF-NMP solution R_{SO} is firstly decreased and then increased. Namely, R_{SO} in the case of $\varphi_{com2} = 0.5\%$ is smaller than that in other cases including $\varphi_{com1} = 0.3\%$, $\varphi_{com3} = 0.7\%$ and $\varphi_{com4} = 0.9\%$. R_{SO} in the cases of both $\varphi_{com1} = 0.3\%$ and $\varphi_{com4} = 0.9\%$ are much larger than that in the case of $\varphi_{com1} = 0.3\%$. In Fig. 6(b), the resistance of the conductive path R_p in the case of $\varphi_{com2} = 0.5\%$ is smaller than that in other cases including $\varphi_{com1} = 0.3\%$, $\varphi_{com3} = 0.7\%$ and $\varphi_{com4} = 0.9\%$. Based on the evolutionary trends of R_{SO} and R_p, a conductive network constructed by the PVDF-composite conductive agent hybrid coating is initially established in the electrode slurry at $\varphi_{com2} = 0.5\%$. As presented in Fig. 6(c),the double-layer resistance R_{dl} of the PVDF - conductive agent composite film decreases first and then increases, whereas the corresponding double-layer capacitance C_{dl} exhibits an opposite variation trend. Namely, R_{dl} and C_{dl} in the case of $\varphi_{com2} = 0.5\%$ is smaller and larger than that in other cases including $\varphi_{com1} = 0.3\%$, $\varphi_{com3} = 0.7\%$ and $\varphi_{com4} = 0.9\%$, respectively. Thus, the variation tendencies of both R_{dl} and C_{dl} illustrate that the PVDF-composite conductive agent double layer structures around $LiCoO_2$ particles with reduced thickness are distributed in LIB slurry in the case of $\varphi_{com2} = 0.5\%$. In comparison with the sample at $\varphi_{com2} = 0.5\%$, reducing the composite conductive agent loading to $\varphi_{com1} = 0.3\%$ renders the PVDF - conductive agent blend insufficient to fully encapsulate particles. This insufficient coating consequently elevates R_{SO}, R_p, R_{dl}, while distinctly lowering C_{dl}, as illustrated in Fig. 6 (d). Simultaneously, compared with $\varphi_{com2} = 0.5\%$, when the amount of composite conductive agent is increased to $\varphi_{com4} = 0.9\%$, a severe excess of the mixture of PVDF and composite conductive agent can cause serious agglomeration of this mixture among different $LiCoO_2$ particles, which also results in the increased R_{SO}, R_p, R_{dl} and the decreased C_{dl} as is shown in Fig. 6.

3.2. Results of LIB slurry with CNTs to Gr mass ratio m_{CNTs}:m_{Gr}

Fig. 7 presents the Nyquist and Bode plots of LIB slurries. All samples were prepared at a fixed composite conductive agent amount of $\varphi_{com2} = 0.5\%$ with six varied CNTs to Gr mass ratios which are m_{CNTs}:$m_{Gr} = 0{:}5$, m_{CNTs}:$m_{Gr} = 1{:}4$, m_{CNTs}:$m_{Gr} = 2{:}3$, m_{CNTs}:$m_{Gr} = 3{:}2$, m_{CNTs}:$m_{Gr} = 4{:}1$ and m_{CNTs}:$m_{Gr} = 5{:}0$. Specifically, in Fig. 7(a), with the increase of m_{CNTs}:m_{Gr}, the semi-circles in both low and high frequency ranges are firstly decreased and then increased. Namely, the semi-circles in the case of m_{CNTs}:$m_{Gr} = 4{:}1$ are smaller than those in the rest cased including m_{CNTs}:$m_{Gr} = 0{:}5$, m_{CNTs}:$m_{Gr} = 1{:}4$, m_{CNTs}:$m_{Gr} = 2{:}3$, m_{CNTs}:$m_{Gr} = 3{:}2$ and m_{CNTs}:$m_{Gr} = 5{:}0$. This indicated that the resistance and reactance of LIB slurry at m_{CNTs}:$m_{Gr} = 4{:}1$ are relatively lower. Based on our previous research (Wang et al., 2019), the low frequency semi-circle corresponds to the dispersion behavior of the PVDF-NMP solution; whereas the high frequency semi-circle reflects the interface dispersion between $LiCoO_2$ particles and NMP solvent. Moreover, in Fig. 7(b), two

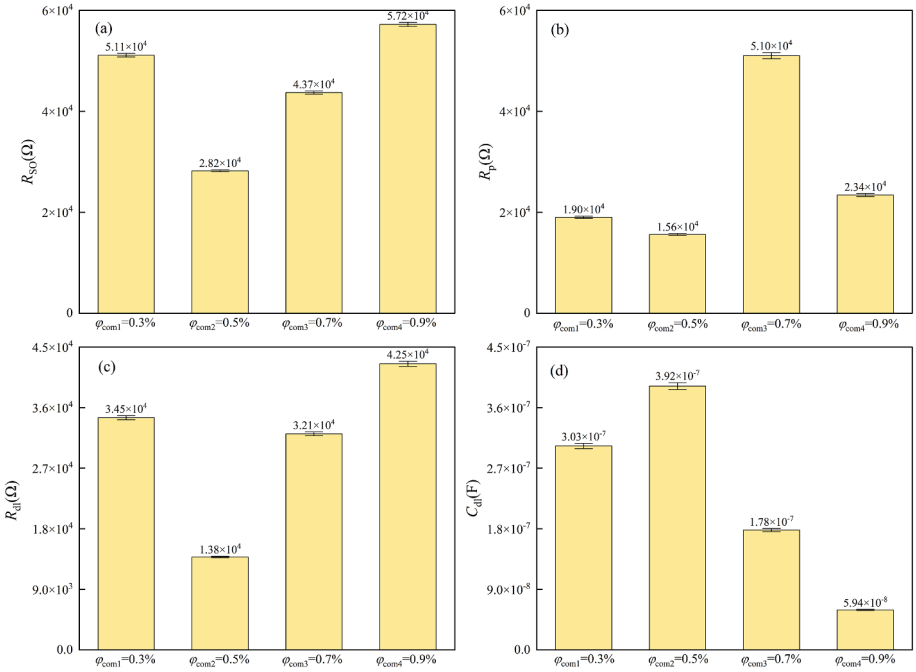

Fig. 6. Fitting results of Nyquist plots for experimental measurement data of LIB slurry under different composite conductive agent content (a) φ_{com1} = 0.3%, (b) φ_{com2} = 0.5%, (c) φ_{com3} = 0.7% and (d) φ_{com4} = 0.9%.

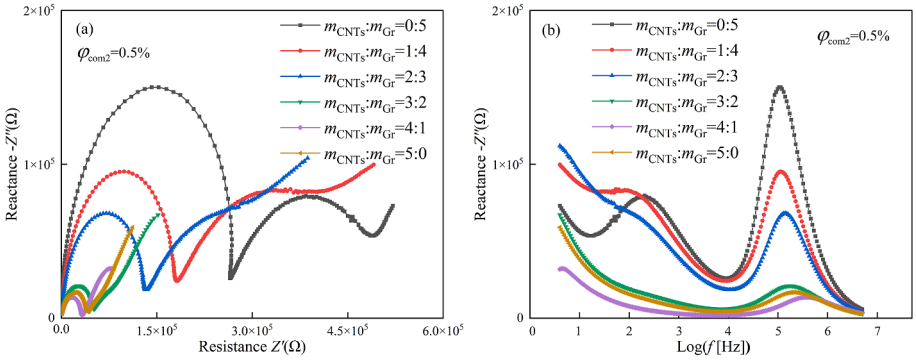

Fig. 7. EIS results of LIB slurry under six different CNTs to Gr mass ratios which are m_{CNTs}:m_{Gr} = 0:5, m_{CNTs}:m_{Gr} = 1:4, m_{CNTs}:m_{Gr} = 2:3, m_{CNTs}:m_{Gr} = 3:2, m_{CNTs}:m_{Gr} = 4:1 and m_{CNTs}:m_{Gr} = 5:0 (a) Nyquist plots (b) Bode plots.

peak frequencies which are peak frequency in high frequency range $f_{peak,\ high}$ and peak frequency in low frequency range $f_{peak,low}$ are appeared in the cases of m_{CNTs}:m_{Gr} = 0:5, m_{CNTs}:m_{Gr} = 1:4 and m_{CNTs}:m_{Gr} = 2:3, while only $f_{peak,\ high}$ is appeared in the cases of m_{CNTs}:m_{Gr} = 3:2, m_{CNTs}:m_{Gr} = 4:1 and m_{CNTs}:m_{Gr} = 5:0. As reported in our previous research (Wang et al., 2025b; 2024), $f_{peak,low}$ characterizes the dispersion frequency of the PVDF–NMP solution, which is closely correlated with particle size. In contrast, $f_{peak,\ high}$ corresponds to the $LiCoO_2$-NMP interfacial dispersion frequency, reflecting the time scale for charge redistribution to reach equilibrium following the removal of external perturbations. Hence, in the cases of m_{CNTs}:m_{Gr} = 0:5, m_{CNTs}:m_{Gr} = 1:4 and m_{CNTs}:m_{Gr} = 2:3, the coexistence of $f_{peak,low}$ and $f_{peak,\ high}$ indicates the presence of composite conductive agent-bare $LiCoO_2$ particles within LIB slurry, while in the cases of m_{CNTs}:m_{Gr} = 3:2, m_{CNTs}:m_{Gr} = 4:1 and m_{CNTs}:m_{Gr} = 5:0, the disappearance of $f_{peak,low}$ denotes that $LiCoO_2$ particles are coated by the mixture of PVDF and composite conductive agent within LIB slurry (Wang et al., 2025b). In order to further analyze the electrical response characteristics of LIB slurry, the variation tendencies of $f_{peak,\ high}$ are shown in Fig. 8. Specifically, $f_{peak,\ high}$ = 4.1 × 10^5 Hz in the case of m_{CNTs}:m_{Gr} = 4:1 is larger than that of

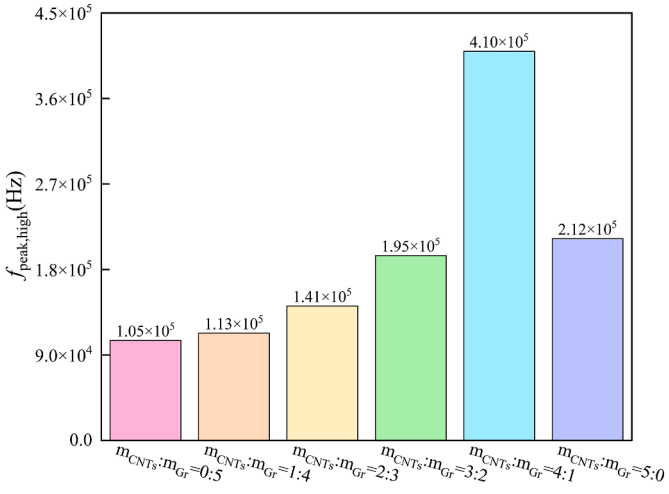

Fig. 8. Peak frequency in the high frequency range $f_{peak,\ high}$ obtained from Fig. 7(b).

other cases including m_{CNTs}:m_{Gr} = 0:5 ($f_{peak,\ high}$ = 1.05 × 10^5 Hz), m_{CNTs}:m_{Gr} = 1:4 ($f_{peak,\ high}$ = 1.13 × 10^5 Hz), m_{CNTs}:m_{Gr} = 2:3 ($f_{peak,\ high}$ = 1.41 × 10^5 Hz), m_{CNTs}:m_{Gr} = 3:2 ($f_{peak,\ high}$ = 1.95 × 10^5 Hz) and m_{CNTs}:m_{Gr} = 5:0 ($f_{peak,\ high}$ = 2.12 × 10^5 Hz). Therefore, a conductive network structure formed by coating the mixture of PVDF and composite conductive agent around $LiCoO_2$ particles is constructed within LIB slurry in the case of m_{CNTs}:m_{Gr} = 4:1.

After using our previously proposed 10-parameter EEC to fit the Nyquist plots of LIB slurries under different m_{CNTs}:m_{Gr}, as is shown in Fig. 9, the electrochemical characteristics of LIB slurry effected by m_{CNTs}:m_{Gr} are able to be obtained. In Fig. 9(a), with the increase of m_{CNTs}:m_{Gr}, R_{SO} is firstly decreased and then increased. Namely, R_{SO} in the case of m_{CNTs}:m_{Gr} = 4:1 is smaller than that of other cases including m_{CNTs}:m_{Gr} = 0:5, m_{CNTs}:m_{Gr} = 1:4, m_{CNTs}:m_{Gr} = 2:3, m_{CNTs}:m_{Gr} = 3:2 and m_{CNTs}:m_{Gr} = 5:0. Meanwhile, in both Fig. 9(b) and (c), the variations of both R_p and R_{dl} are that they first increased sharply, then decreased rapidly, followed by a slight increase. Specifically, both R_p and R_{dl} in the case of m_{CNTs}:m_{Gr} = 4:1 are also smaller than that of other cases including m_{CNTs}:m_{Gr} = 0:5, m_{CNTs}:m_{Gr} = 1:4, m_{CNTs}:m_{Gr} = 2:3, m_{CNTs}:m_{Gr} = 3:2 and m_{CNTs}:m_{Gr} = 5:0. Furthermore, in Fig. 9(d), C_{dl} in the case of m_{CNTs}:m_{Gr} = 4:1 is larger than that of other cases which are m_{CNTs}:m_{Gr} = 0:5, m_{CNTs}:m_{Gr} = 1:4, m_{CNTs}:m_{Gr} = 2:3, m_{CNTs}:m_{Gr} = 3:2 and m_{CNTs}:m_{Gr} = 5:0. To sum up, smaller R_{SO} and R_p show that a conductive network structure is well formed by the mixture of PVDF and composite conductive agent around $LiCoO_2$ particles, meanwhile, smaller R_{dl} and larger C_{dl} lead to the fact that the thinner PVDF-composite conductive agent double-layer structure enables more uniform dispersion of $LiCoO_2$ particles coated by the mixture of PVDF-composite conductive agent. Therefore, a well dispersed conductive network structure is formed within LIB slurry in the cases of φ_{com2} = 0.5% and m_{CNTs}:m_{Gr} = 4:1.

Nevertheless, when compared the effects of the single conductive agents in the cases of m_{CNTs}:m_{Gr} = 0:5 and m_{CNTs}:m_{Gr} = 5:0 and the composite conductive agent in the case m_{CNTs}:m_{Gr} = 4:1, it can be easily observed that LIB slurry with the single conductive agent which is CNTs or Gr has larger R_{SO} & R_p as well as smaller $f_{peak,\ high}$ & C_{dl}, while LIB slurry with composite conductive agent which is composed of both CNTs and Gr has smaller R_{SO} & R_p as well as larger $f_{peak,\ high}$ & C_{dl}. The above-mentioned variation tendencies of each parameter can be well explained by the following two reasons. Firstly, single CNTs exhibit a high aspect ratio and predominantly present a filamentous entangled agglomeration morphology at the microscopic scale, leading to challenges in achieving uniform dispersion during the dispersion process and insufficient interfacial contact with $LiCoO_2$ active materials (Wang et al., 2017). This leads to the "short-range" conductive pathways constructed by the mixture of PVDF and slightly aggregated single CNTs around $LiCoO_2$ particles in LIB slurry. Secondly, in contrast, single Gr exhibits a large specific surface area and high density, with its structure predominantly consisting of multi-layered flake-like architectures. Despite its excellent coating capability and interfacial connectivity with active materials, Gr possesses inadequate structural support capacity and is prone to re-agglomeration subsequent to the dispersion (Shi et al., 2019). This also results in the "short-range" conductive pathways constructed by the mixture of PVDF and seriously aggregated single Gr around $LiCoO_2$ particles in LIB slurry. Herein, by separately comparing the "short--range" conductive pathways constructed by single CNTs and single Gr in LIB slurry, the results presented in Figs. 7–9 are all consistent with the deduced conclusion. This further validates the correctness of our inference that single CNTs undergo slight agglomeration, whereas single Gr exhibits severe agglomeration in LIB slurry. Thus, although CNTs possess prominent inherent longitudinal supporting capability and can construct long-range conductive pathways, single-component CNTs are also capable of forming "short-range" conductive pathways in LIB slurry. To fully leverage the advantage of CNTs in establishing "long-range" conductive networks, it is necessary to compound CNTs with Gr to prepare composite conductive agents. In fact, CNTs predominantly exhibit excellent inherent longitudinal structural support and outstanding capability to construct "long-range" conductive pathways, while Gr possesses distinct advantages in building "short-range" conductive pathways with a prominent wrapping effect (Peng et al., 2024; Shen et al., 2011). Accordingly, the fabrication of CNTs/Gr composite conductive agents can not only compensate for their respective inherent defects in conductive network construction, but also allow long tubular CNTs to provide structural support for sheet-like graphene, effectively alleviating the agglomeration tendency of Gr nanosheets.

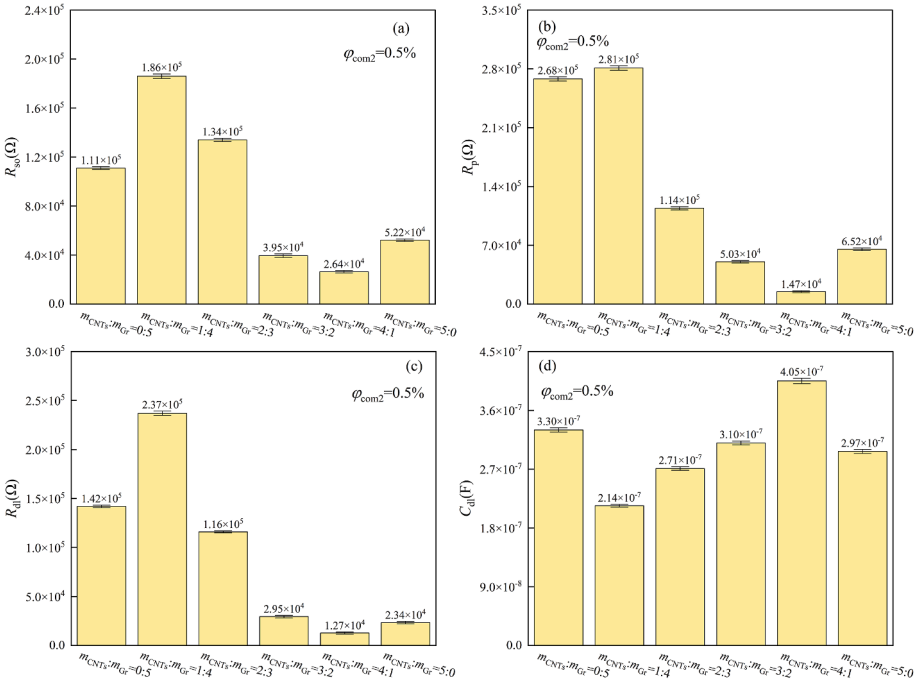

Fig. 9. Fitting results of Nyquist plots for experimental measurement data of LIB slurry under six different CNTs to Gr mass ratios (a) R_{so} (b) R_p (c) R_{dl} (d) C_{dl}.

4. Discussion of dispersion characterizations of LIB slurry

4.1. Morphological characterizations of LIB slurry

Based on the EIS results shown from Figs. 4–6, it is able to know that the internal structure of LIB slurry in the case of $\varphi_{com2} = 0.5\%$ is better than that in the case of $\varphi_{com4} = 0.9\%$. Thus, the SEM image in the case of $\varphi_{com2} = 0.5\%$ is compared with that in the case of $\varphi_{com4} = 0.9\%$ in Fig. 10. In Fig. 10(a), it is clear that $LiCoO_2$ particles are coated by the mixture of PVDF and CNTs-Gr composite conductive agent, meanwhile, different dispersed $LiCoO_2$ particles are connected by the mixture of PVDF and CNTs. This is caused by the synergistic effect between CNTs and Gr in LIB slurry (Li et al., 2015). In Fig. 10(b), CNTs and Gr are seriously aggregated in local regions although all $LiCoO_2$ particles are coated by the mixture of PVDF and CNTs-Gr composite conductive agent. Specifically, excessive CNTs and Gr form a large number of agglomerates when forming composite conductive agent. On one hand, excessive CNTs agglomerate into spherical particles, which is difficult to support Gr, on the other hand, excessive Gr is extremely easy to form large-area flaky agglomerates, which undoubtedly increased the impedance of LIB slurry. The above-mentioned internal structures of LIB slurry shown in Fig. 10(a) and (b) are consistent with those deduced from Figs. 4–6, which verified the correctness of the electrochemical characterizations of LIB slurry when considered the influence factor of composite conductive agent amount.

Under the optimal condition that $\varphi_{com2} = 0.5\%$ is determined, considering the mass ratio of CNTs to Gr m_{CNTs}:m_{Gr} in composite conductive agent becomes more critical. According to the EIS results shown from Figs. 7–9, it is obvious that the internal structure of LIB slurry in the case of m_{CNTs}:$m_{Gr} = 4{:}1$ is much better that that in the case of m_{CNTs}:$m_{Gr} = 1{:}4$. In order to also verify the correctness of these electrochemical characterizations of LIB slurry, it is essential to use the direct observation approach for analyzing the apparent morphological characterizations based on the SEM images of LIB slurry. Thus, based on the SEM experiment, as is shown in Fig. 11, SEM images of LIB slurry under the conditions of m_{CNTs}:$m_{Gr} = 4{:}1$ and m_{CNTs}:$m_{Gr} = 1{:}4$ are presented. In Fig. 11(a), large-volume $LiCoO_2$ particles coated by the mixture of PVDF and composite conductive agent are well dispersed to form a conductive network structure in LIB slurry, meanwhile, the main function of composite conductive agent composed of CNTs and Gr is to connect adjacent different $LiCoO_2$ particles with the aim of providing much more conductive paths for electrons. In Fig. 11(b), $LiCoO_2$ particles are partly coated by the mixture of PVDF and composite conductive agent, meanwhile, Gr is seriously aggregated in LIB slurry, while CNTs are not enough to form the conductive paths. Concretely, in the case of m_{CNTs}:$m_{Gr} = 4{:}1$, on one side, the flaky Gr is tightly coated on the surface of $LiCoO_2$; on the other side, the long tubular CNTs longitudinally support part of Gr and connect it with another $LiCoO_2$ particle wrapped by Gr like tentacles. The above-mentioned internal structures of LIB slurry shown in Fig. 11(a) and (b) are consistent with those deduced from Figs. 7–9, which verified the correctness of the electrochemical characterizations of LIB slurry when considered the influence factor of the mass ratio of CNTs to Gr m_{CNTs}:m_{Gr}.

To quantitatively assess the SEM micrographs in Figs. 10 and 11, the dispersion degrees of $LiCoO_2$ particles and composite conductive agent were systematically calculated. According to our previous research (Wang et al., 2025a), the mixed attention module-enhanced Mask R-CNN was utilized for $LiCoO_2$ particle recognition, and the corresponding identification results are presented in Fig. 12. Meanwhile, the differential shadow method was adopted to eliminate identified $LiCoO_2$ regions from slurry SEM images and extract grayscale images of composite conductive agents (Jha et al., 2022). The hybrid OTSU–Niblack algorithm was further applied to determine the optimal threshold for global binarization (Athimethphat, 2011), converting the acquired grayscale images into binary images, as illustrated in Fig. 13. Consequently, Table 3 shows the quantitative evaluation results for both $LiCoO_2$ and composite conductive agent dispersion degree in LIB slurry under four different conditions. Specifically, regarding the dispersion degree of $LiCoO_2$ particles, the sample with m_{CNTs}:$m_{Gr} = 4{:}1$ exhibits notably higher dispersed particle proportion ($\eta = 14.9\%$) and average minimum distance ($S_{min} = 6.1$ μm) than other formulations. For comparison, representative parameters are $\eta = 7.40\%$ & $S_{min} = 5.70$ μm at $\varphi_{com2} = 0.5\%$, $\eta = 4.75\%$ & $S_{min} = 5.07$ μm at $\varphi_{com4} = 0.9\%$, and $\eta = 6.30\%$ & $S_{min} = 5.06$ μm at m_{CNTs}:$m_{Gr} = 1{:}4$. Meanwhile, this m_{CNTs}:$m_{Gr} = 4{:}1$ sample delivers a much lower uniformity deviation $\beta = 2.38$, which is far below the values of reference samples: $\beta = 4.71$ ($\varphi_{com2} = 0.5\%$), $\beta = 10.23$ ($\varphi_{com4} = 0.9\%$), $\beta = 12.03$ (m_{CNTs}:$m_{Gr} = 1{:}4$). In terms of composite conductive agent dispersion degree, the m_{CNTs}:$m_{Gr} = 4{:}1$ sample achieves a higher η of 2.81%, exceeding those of the control samples ($\eta = 2.26\%$ for $\varphi_{com2} = 0.5\%$, $\eta = 1.48\%$ for $\varphi_{com4} = 0.9\%$ and $\eta = 0.34\%$ for m_{CNTs}:$m_{Gr} = 1{:}4$). Correspondingly, the m_{CNTs}:$m_{Gr} = 4{:}1$ sample's $\beta = 6.91 \times 10^2$ is also markedly reduced compared with other conditions, including $\beta = 8.81 \times 10^2$ ($\varphi_{com2} = 0.5\%$), $\beta = 1.21 \times 10^3$($\varphi_{com4} = 0.9\%$), $\beta = 1.40 \times 10^3$ (m_{CNTs}:$m_{Gr} = 1{:}4$). Therefore, LIB slurry with m_{CNTs}:$m_{Gr} = 4{:}1$ exhibits higher η and S_{min} as well as a lower β. Such quantitative results demonstrate that both $LiCoO_2$ particles and composite conductive agent are well dispersed within LIB slurry, thereby forming a continuous network structure within LIB slurry. Collectively, this finding aligns with the slurry dispersion behavior illustrated in Figs. 6 and 9, which further confirms the reliability of the earlier EIS interpretation.

4.2. Stability characterizations of LIB slurry

Besides the apparent morphological characterizations, the stability characterizations of LIB slurry are also another critical factor for evaluating its dispersion performance. As shown in Fig. 14, after standing for 7 days, all LIB slurry samples exhibit stratification into a supernatant layer and a turbid bottom layer. Specifically, Fig. 14(a) and (b) show the photographic images of LIB slurry with different composite conductive

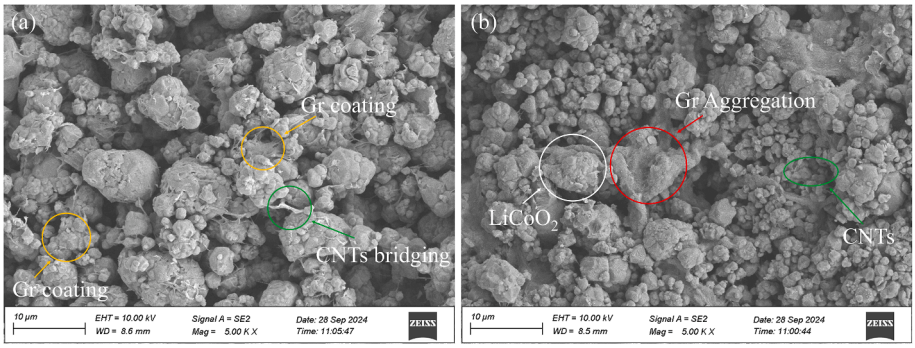

Fig. 10. SEM images of LIB slurry under different conditions (a) $\varphi_{com2} = 0.5\%$ (b) $\varphi_{com4} = 0.9\%$.

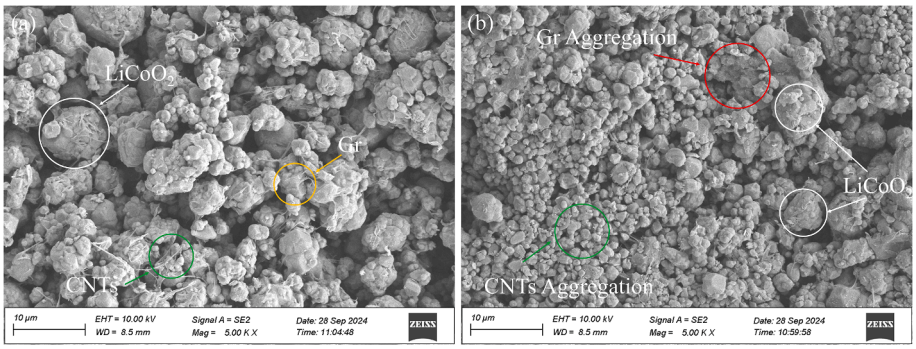

Fig. 11. SEM images of LIB slurry under different conditions (a) m_{CNTs}:m_{Gr} = 4:1 (b) m_{CNTs}:m_{Gr} = 1:4.

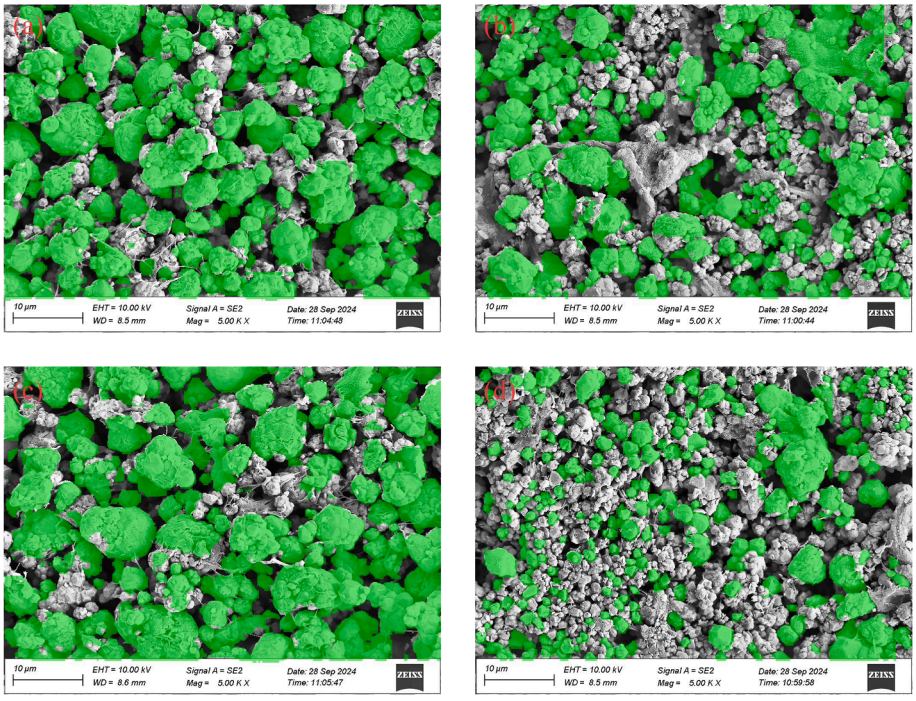

Fig. 12. Identified images of $LiCoO_2$ particles based on SEM images under different conditions (a) φ_{com2} = 0.5% (b) φ_{com4} = 0.9% (c) m_{CNTs}:m_{Gr} = 4:1 and (d) m_{CNTs}:m_{Gr} = 1:4.

agent amount before and after sedimentation process, respectively. In Fig. 14(a), the initial liquid level heights of LIB slurries are all consistent under two different composite conductive agent amounts which are φ_{com2} = 0.5% and φ_{com4} = 0.9%. However, as is shown in Fig. 14(b), after GS experiments, owing to gravity, particles in the slurry are capable of settling even in a high-viscosity colloidal suspension, resulting in the stratification of the liquid level in LIB slurry. When LIB slurry undergoes stratification, the supernatant is PVDF-NMP solution, the turbid bottom layer remains an opaque high-viscosity colloidal suspension. In particular, the supernatant height of LIB slurry in the case of φ_{com2} = 0.5% is lower than that in the cases of φ_{com4} = 0.9%. Additionally, Fig. 14(c) and (d) show the photographic images of LIB slurry sedimentation process with different CNTs to Gr mass ratio m_{CNTs}:m_{Gr} before and after sedimentation process, respectively. Similar to Fig. 14 (a) and (c) also presents the initial liquid level heights of LIB slurries under two different the mass ratio of CNTs to Gr m_{CNTs}:m_{Gr} which are m_{CNTs}:m_{Gr} = 4:1 and m_{CNTs}:m_{Gr} = 1:4. Simultaneously, as shown in Fig. 14(d), the supernatant height of LIB slurry in the case of m_{CNTs}:m_{Gr} = 4:1 is lower than that in the case of m_{CNTs}:m_{Gr} = 1:4.

In order to quantitatively evaluate the sedimentation phenomenon of LIB slurry, the average sedimentation rate V and sedimentation ratio are defined as follows:

$$V = \frac{H_0 - H_t}{t} \tag{1}$$

$$Y = \frac{H_{final}}{H_0} \tag{2}$$

Herein, H_0 denotes the initial volume-related height, H_t refers to the volume-related height of the lower turbid liquid at time t. Besides, H_{final} denotes the final volume-related height of the lower turbid liquid after complete sedimentation. Fig. 15 illustrates the variation of V for GS experiments under different conditions. In Fig. 15(a), V=0.088ml/24h in the case of φ_{com2} = 0.5% is lower than V=0.148ml/24h in the case of φ_{com4} = 0.9%. This demonstrates that in the case that composite conductive agent amount is relatively higher (φ_{com4} = 0.9%), V tends to be faster because of the aggregated composite conductive agent. In contrast, in the case that composite conductive agent is added at an appropriate content (φ_{com2} = 0.5%), the dispersion stability of LIB slurry is relatively good, which leads to the slow sedimentation rate of particles. In Fig. 15(b), V=0.071ml/24h in the case of m_{CNTs}:m_{Gr} = 4:1 is also lower than V=0.106ml/24h in the case of m_{CNTs}:m_{Gr} = 1:4. This shows

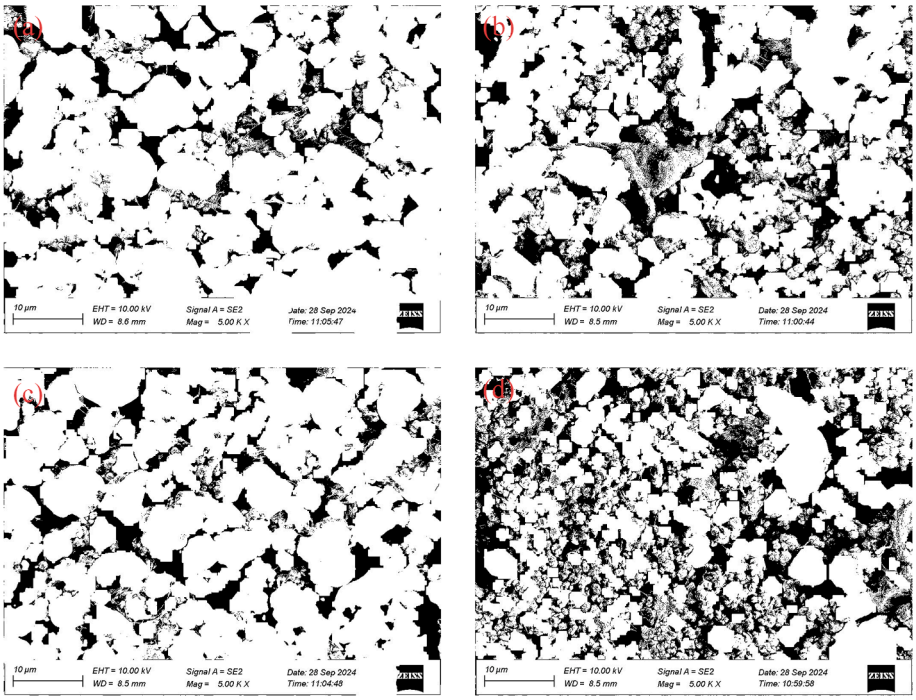

Fig. 13. Identified images of composite conductive agent based on SEM images under different conditions (a) $\varphi_{com2} = 0.5\%$ (b) $\varphi_{com4} = 0.9\%$ (c) m_{CNTs}:m_{Gr} = 4:1 and (d) m_{CNTs}:m_{Gr} = 1:4.

Table 3
Quantitative evaluation results for both $LiCoO_2$ and composite conductive agent dispersion degree in LIB slurry under different conditions.

Figs. 11 and 12 images at different conditions	$LiCoO_2$ dispersion degree			Composite conductive agent dispersion degree	
	Proportion of dispersed particles η	Average mini. distance S_{min}	Uniformity deviation value β	Proportion of dispersed particles η	Uniformity deviation value β
(a) $\varphi_{com2} = 0.5\%$	7.40%	5.70 μm	4.71	2.26%	8.81×10^2
(b) $\varphi_{com4} = 0.9\%$	4.75%	5.07 μm	10.23	1.48%	1.21×10^3
(c) m_{CNTs}:m_{Gr} = 4:1	14.9%	6.10 μm	2.38	2.81%	6.91×10^2
(d) m_{CNTs}:m_{Gr} = 1:4	6.30%	5.06 μm	12.03	0.34%	1.40×10^3

that when the proportion of CNTs in the composite conductive agent is higher, its supporting effect on Gr is better, thereby enhancing the internal structural stability of LIB slurry. Simultaneously, when the proportion of CNTs is lower, the supporting effect of CNTs is insufficient, leading to increased agglomeration of the composite conductive agent and a poor dispersion effect, thereby resulting in a higher sedimentation rate of LIB slurry. Therefore, under the conditions of both $\varphi_{com2} = 0.5\%$ and m_{CNTs}:m_{Gr} = 4:1, through the synergistic effect of CNTs and Gr, the composite conductive agent can more effectively coat and interconnect $LiCoO_2$ particles. The formed three-dimensional conductive network structure is capable of maintaining the stability of its internal skeleton structure during the sedimentation process of LIB slurry.

Fig. 16 illustrates the variation of Y for GS experiments under different conditions. In Fig. 16(a), Y with different composite conductive agent amount presents a slight upward then downward trend with the increase of additive dosage. The slurry prepared at $\varphi_{com2} = 0.5\%$ delivers a higher sedimentation ratio compared with the samples at $\varphi_{com1} = 0.3\%$, $\varphi_{com3} = 0.7\%$ and $\varphi_{com4} = 0.9\%$. This demonstrates that CNTs can provide robust vertical support for Gr at $\varphi_{com2} = 0.5\%$, thereby maintaining the stability of the LIB slurry. As shown in Fig. 16(a) and (b), the Y value of 0.988 at m_{CNTs}:m_{Gr} = 4:1 is greater than those of 0.961 ($\varphi_{com2} = 0.5\%$) and 0.954 (m_{CNTs}:m_{Gr} = 1:4). Therefore, the synergistic combination of CNTs and Gr in the case of m_{CNTs}:m_{Gr} = 4:1 enables effective encapsulation and connection of active particles to form three-dimensional network, which maintains the stability of the internal skeleton structure of LIB slurry during sedimentation.

5. Conclusions

The dispersion characterizations of LIB slurry are investigated under the influences of both composite conductive agent amount φ_{com} and CNTs to Gr mass ratio m_{CNTs}:m_{Gr}. Three techniques including EIS, SEM and GS are applied to characterize the electrochemical characterizations, apparent morphology characterizations and structural stability, which further clarifies the dispersion characterizations of LIB slurry. Four different composite conductive agent amounts which are $\varphi_{com1} = 0.3\%$, $\varphi_{com2} = 0.5\%$, $\varphi_{com3} = 0.7\%$ and $\varphi_{com4} = 0.9\%$ and six different CNTs to Gr mass ratios which are m_{CNTs}:m_{Gr} = 0:5, m_{CNTs}:m_{Gr} = 1:4, m_{CNTs}:m_{Gr} = 2:3, m_{CNTs}:m_{Gr} = 3:2, m_{CNTs}:m_{Gr} = 4:1 and m_{CNTs}:m_{Gr} = 5:0 are selected. In EIS experiment, a reported 10-parameter EEC is used to fit the Nyquist plots derived from experimental data. Meanwhile, for SEM characterization, a previously developed Mask R-CNN algorithm integrated with a mixed attention module was adopted to conduct quantitative morphological analysis. By integrating EIS, SEM and GS results, key conclusions concerning LIB slurry dispersion properties are summarized below:

(1) As the amounts of composite conductive agents varies from $\varphi_{com1} = 0.3\%$ to $\varphi_{com4} = 0.9\%$, the impedance of LIB slurry decreases initially and then increases. Electrochemical,

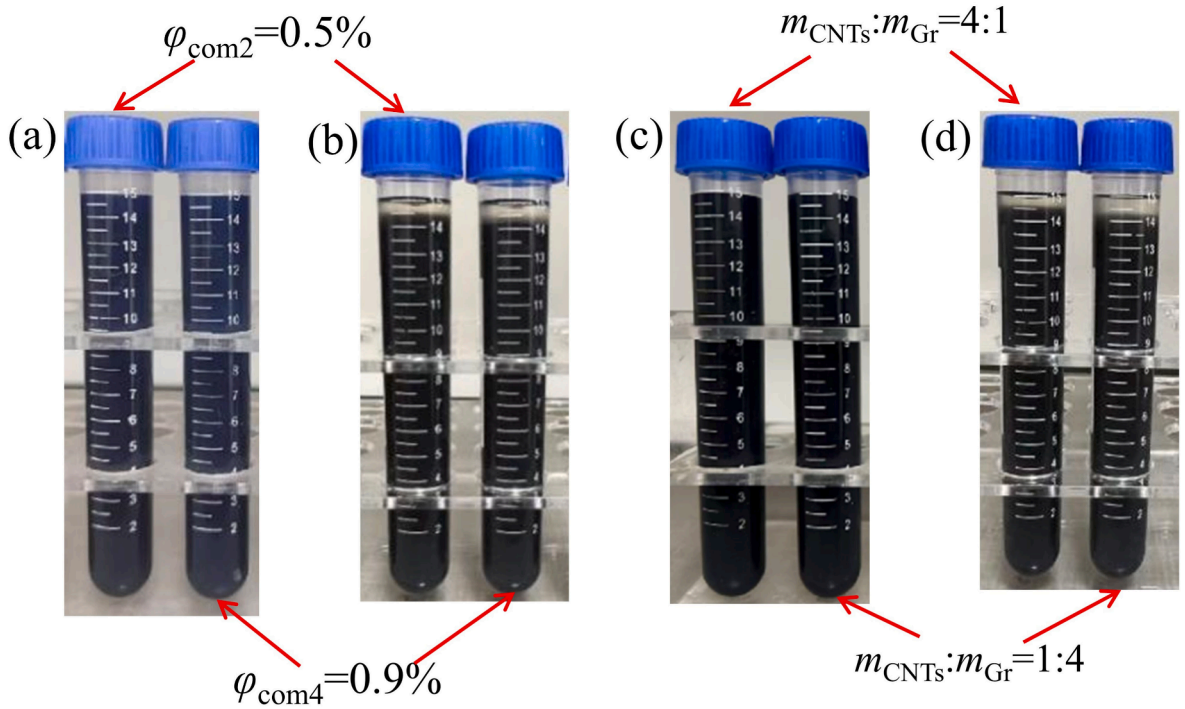

Fig. 14. Experimental results of GS for LIB slurry (a) initial state affected by composite conductive agent amount, (b) final state affected by composite conductive agent amount, (c) initial state affected by the mass ratio of CNTs to Gr (d) final state affected by the mass ratio of CNTs to Gr.

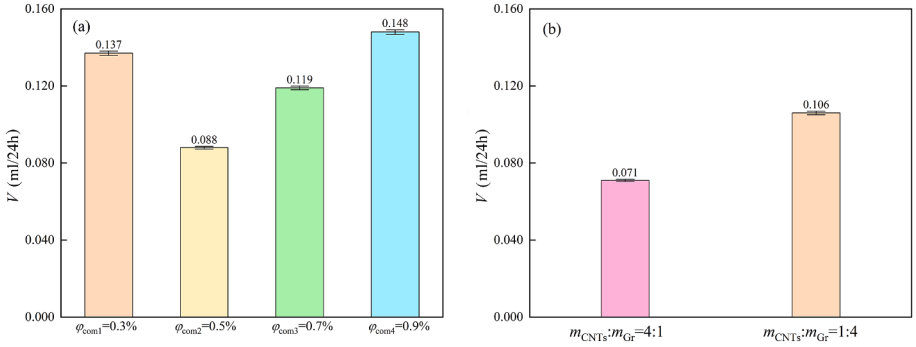

Fig. 15. Quantitative evaluation results of GS experiments (a) sedimentation rate *V* effected by composite conductive agent amount (b) sedimentation rate *V* effected by the mass ratio of CNTs to Gr.

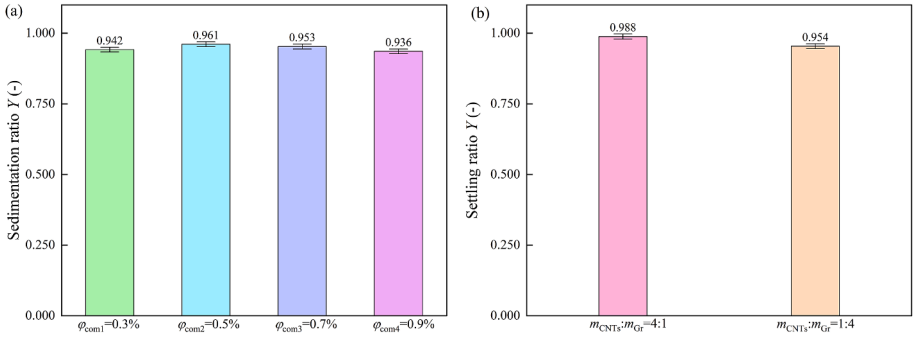

Fig. 16. Quantitative evaluation results of GS experiments (a) sedimentation ratio *Y* effected by composite conductive agent amount (b) sedimentation ratio *Y* effected by the mass ratio of CNTs to Gr.

morphological and sedimentation characterization verifies the optimal dispersion state at $\varphi_{com2} = 0.5\%$. The PVDF-based composite conductive agent encapsulates and interconnects $LiCoO_2$ particles, with its bilayer structure uniformly distributed around $LiCoO_2$ particle surfaces. This unique microstructure enables homogeneous dispersion of $LiCoO_2$ particles in LIB slurry.

(2) When altering the mass ratio of CNTs to Gr from m_{CNTs}:m_{Gr} = 0:5 to m_{CNTs}:m_{Gr} = 5:0, the electrical impedance of LIB slurry undergoes an initial decrease followed by an increase. Combined electrochemical, morphological and sedimentation analyses confirm the optimal dispersion performance at m_{CNTs}:m_{Gr} = 4:1. It is concluded that the thin bilayer structure of the PVDF-composite conductive agent not only achieves effective coating of $LiCoO_2$ particles, but also enables excellent homogeneous dispersion of both active $LiCoO_2$ particles and CNTs/Gr composite conductive agents within LIB slurry.

(3) The "short-range" conductive pathways are respectively constructed by PVDF blended with slightly dispersed individual CNTs and severely aggregated pristine Gr around $LiCoO_2$ particles in LIB slurry. To fully leverage the superior longitudinal structural support of CNTs and the excellent wrapping effect of Gr, the CNTs/Gr composite conductive agent prepared under the conditions of φ_{com2} = 0.5% and m_{CNTs}:m_{Gr} = 4:1 can compensate for the inherent shortcomings of individual CNTs and pristine Gr alone, thereby establishing efficient "long-range" conductive networks in LIB slurry.

Therefore, this work establishes a solid experimental basis, which holds great potential for optimizing the comprehensive performance of LIBs.

CRediT authorship contribution statement

Zhilong Wang: Methodology, Investigation, Conceptualization. **Bingjia Li:** Writing – original draft. **Xiao Yang:** Writing – original draft. **Jianhang Lu:** Formal analysis, Data curation. **Jiatan Zhang:** Methodology. **Chunguo Zhou:** Formal analysis. **Irfan Bahiuddin:** Supervision, Project administration. **Bo Sun:** Investigation, Data curation. **Tong Zhao:** Writing – review & editing, Supervision.

Declaration of competing interest

The authors declare that they have no known competing financial interests or personal relationships that could have appeared to influence the work reported in this paper.

Acknowledgement

We would like to thank the support from the program of the International Scientific and Technological Cooperation Promotion Program of Xi'an University of Technology (grant No. 2024GHCJ007). Thanks for the experimental and simulation data provided by Mr Yinhao Yu of Xi'an University of Technology.

References

An, H., Jiang, L., Li, F., Wu, P., Zhu, X., Wei, S., & Zhou, Y. (2020). Hydrogel-derived three-dimensional porous Si-CNT@ G nanocomposite with high-performance lithium storage. *Acta Physico-Chimica Sinica, 36*, Article 1905034.

Athimethphat, M. (2011). A review on global binarization algorithms for degraded document images. *AU JT, 14*(3), 188–195.

Cao, M., Wang, L., Zhang, Q., Zhang, H., Zhong, S., & Chen, J. (2023). Boosting the comprehensive behaviors of LiNi0.5Co0.2Mn0.3O2 lithium-ion batteries via CNTs/Super-P composite conductive agent. *Materials Today Communications, 36*, Article 106677.

Chen, Y. T., Zhang, H. Y., Chen, Y. M., Qin, G., Lei, X. L., & Liu, L. Y. (2018). Graphene-carbon nanotubes-modified LiFePO4 cathode materials for high-performance lithium-ion batteries. *Materials Science Forum, 913,* 818–830.

Chen, K., Zhang, D., Shen, X., Feng, X., Cheng, X., & Wu, Y. (2026). Emerging thermal safety characteristics of large-capacity Lithium Iron phosphate lithium-ion batteries. *Advanced Energy Materials, 16*(1), Article e03248.

Ding, D., Maeyoshi, Y., Kubota, M., Wakasugi, J., Kanamura, K., & Abe, H. (2020). Holey reduced graphene oxide/carbon nanotube/LiMn0. 7Fe0. 3PO4 composite cathode for high-performance lithium batteries. *Journal of Power Sources, 449*, Article 227553.

Fan, J., & Fedkiw, P. S. (1998). Electrochemical impedance spectra of full cells: Relation to capacity and capacity-rate of rechargeable Li cells using LiCoO , LiMn O , and 2 2 4 LiNiO cathodes. *Journal of Power Sources, 72*, 165–173. https://doi.org/10.1016/S0378-7753(97)02708-0

Ikeno, N., Prayitno, Y. A. K., Sejati, P. A., Kawashima, D., & Takei, M. (2022). In situ 4D distribution visualization of carbon-black volume fraction in cathode slurry of lithium-ion battery by multi-layered electrical resistance tomography (mlERT). *Advanced Powder Technology, 33*(10), Article 103766.

Jha, A., Singh, A., Ali, A. B., & Jindal, R. (2022). Character segmentation on Indian vehicle license plate using K-means, OTSU and niblack algorithm. In *2022 third international conference on intelligent computing instrumentation and control technologies (ICICICT)* (pp. 893–897).

Kim, J., Song, S., Lee, C. S., Lee, M., & Bae, J. (2023). Prominent enhancement of stability under high current density of LiFePO4-based multidimensional nanocarbon composite as cathode for lithium-ion batteries. *Journal of Colloid and Interface Science, 650*, 1958–1965.

Lei, X., Zhang, H., Chen, Y., Wang, W., Ye, Y., Zheng, C., Deng, P., & Shi, Z. (2015). A three-dimensional LiFePO4/carbon nanotubes/graphene composite as a cathode material for lithium-ion batteries with superior high-rate performance. *Journal of Alloys and Compounds, 626*, 280–286.

Lei, X., Zhang, H., Chen, Y., Wang, W., Ye, Y., Zheng, C., … Shi, Z. (2015). A three-dimensional LiFePO4/carbon nanotubes/graphene composite as a cathode material for lithium-ion batteries with superior high-rate performance. *Journal of Alloys and Compounds: An Interdisciplinary Journal of Materials Science and Solid-State Chemistry and Physics, 626*, 280–286.

Li, X., Zhang, X., Li, T., Zhong, Q., Zhang, Y., & Huang, J. (2015). Effects of nano carbon conductive additives on the electrochemical performance of LiCoO 2 cathode for Lithium Ion batteries. *Journal of New Materials for Electrochemical Systems, 18*(3), 131–135. https://doi.org/10.14447/jnmes.v18i3.358

Liu, A., Yu, S., Lu, X., & Liu, S. (2023). Confining NiCo2O4 nanoparticles in nitrogen doped carbon nanotubes embedded in 3D porous graphene aerogels for superior lithium storage. *Journal of Electroanalytical Chemistry, 942*, Article 117565.

Liu, Y., Zhang, H., Huang, Z., Wang, Q., Guo, M., Zhao, M., Zhang, D., Wang, J., He, P., & Liu, X. (2022). Understanding the influence of nanocarbon conducting modes on the rate performance of LiFePO4 cathodes in lithium-ion batteries. *Journal of Alloys and Compounds, 905*, Article 164205.

Liu, G., Zheng, H., Simens, A. S., Minor, A. M., Song, X., & Battaglia, V. S. (2007). Optimization of acetylene black conductive additive and PVDF composition for high-power rechargeable lithium-ion cells. *Journal of the Electrochemical Society, 154*(12), A1129–A1134.

Peng, R., Jiang, T., Luo, Q., Li, L., & Chen, J. (2024). CNTs/Gr composite sandwich layered rare earth phthalocyanines MPcs (M= Yb, La) used as improved energy storage behaviors for lithium-ion batteries. *Journal of Energy Storage, 99*, Article 113328.

Shen, L., Zhang, X., Li, H., Yuan, C., & Cao, G. (2011). Design and tailoring of a three-dimensional TiO2–graphene–carbon nanotube nanocomposite for fast lithium storage. *Journal of Physical Chemistry Letters, 2*(24), 3096–3101.

Shi, Y., Wen, L., Pei, S., Wu, M., & Li, F. (2019). Choice for graphene as conductive additive for cathode of lithium-ion batteries. *Journal of Energy Chemistry, 30*, 19–26.

Wang, Z., Lu, J., Zhang, J., Li, F., Sun, B., Zhao, T., & Bahiuddin, I. (2025a). Quantitative evaluation of particle distribution status of lithium-ion battery (LIB) slurry under effects of rotational speeds. *Particuology*.

Wang, Z., Lu, J., Zhang, J., Li, F., Yu, X., Sun, B., Cui, Y., & Zhao, T. (2025b). Clarification of network structure of lithium-ion battery slurry under effects of composite conductive agent amount and carbon black to graphene mass ratio. *Particuology*.

Wang, Z., Tu, J., Yu, X., Li, F., Zhao, Z., Cui, Y., & Zhao, T. (2024). Optimization of mixing speed and time to disperse the composite conductive agent composed of carbon black and graphene in lithium-ion battery slurry. *Particuology, 92*, 1–12.

Wang, M.-S., Wang, Z.-Q., Yang, Z.-L., Huang, Y., Zheng, J., & Li, X. (2017). Carbon nanotube-graphene nanosheet conductive framework supported SnO2 aerogel as a high performance anode for lithium ion battery. *Electrochimica Acta, 240*, 7–15.

Wang, Z., Zhao, T., & Takei, M. (2017b). Morphological structure characterizations in lithium-ion battery (LIB) slurry under shear rotational conditions by on-line dynamic electrochemical impedance spectroscopy (EIS) method. *Journal of the Electrochemical Society, 164*(9), A2268.

Wang, Z., Zhao, T., & Takei, M. (2019). Clarification of particle dispersion behaviors based on the dielectric characteristics of cathode slurry in lithium-ion battery (LIB). *Journal of the Electrochemical Society, 166*(2), A35–A46.

Wang, Z., Zhao, T., Yao, J., Kishikawa, Y., & Takei, M. (2017a). Evaluation of the electrochemical characterizations of lithium-ion battery (LIB) slurry with 10-Parameter Electrical Equivalent Circuit (EEC). *Journal of the Electrochemical Society, 164*(2), A8–A17.

Zeng, S., Li, Y., Peng, J., He, Z., Liang, Z., Xu, W., Lan, L., & Liang, X. (2025). Optimization design of conductive agent based on ternary lithium-ion battery. *Energy Storage Science and Technology, 14*(3), 1187.

Zhang, J., Yu, M., Li, S., Meng, Y., Wu, X., & Liu, J. (2016). Transparent conducting oxide-free nitrogen-doped graphene/reduced hydroxylated carbon nanotube composite paper as flexible counter electrodes for dye-sensitized solar cells. *Journal of Power Sources, 334*, 44–51.

Zhang, Q., Zhang, Y., Yin, Y., Fan, L., & Zhang, N. (2020). Packing FeF3· 0.33 H2O into porous graphene/carbon nanotube network as high volumetric performance cathode for lithium ion battery. *Journal of Power Sources, 447*, Article 227303.

Zheng, M., You, Y., & Lu, J. (2025). Understanding materials failure mechanisms for the optimization of lithium-ion battery recycling. *Nature Reviews Materials, 10*(5), 355–368.